Copper oxide-water nanofluid flow within an annulus shaped cavity: A numerical study on natural convective heat transfer

M. J. Uddin*, M. A. Halim, M. Mohiuddin, Shalauddin

Faculty of Science and Information Technology, Daffodil International University, Dhaka, Bangladesh

jashim.fluidm@gmail.com

ABSTRACT. *The purpose of the study is to investigate the heat transfer for copper oxide-water nanofluid flow inside a concentrical annulus between a colder square and het up elliptical cylinder using nonhomogeneous dynamic model numerically. The uniform temperature is applied for the elliptic cylinder and square wall. An unvarying magnetic field is enforced within an enclosure. The momentum, energy and concentration equations along with the continuity equations of nanofluids are strongly coupled and nonlinear and solved using the Galerkin finite element method. The flow, thermal and concentration fields have been displayed to recognize the heat transfer for copper oxide-water nanofluid. The nature of the heat transfer is justified for pertinent parameters of the problem. The results show that the flow, thermal field, and concentration field are strongly controlled by the applied magnetic field. The heat transfer increases significantly for the increase of nanoparticle volume fraction, thermal Rayleigh number and slightly for the magnetic field inclination angle whereas it decreases remarkably for an increase of the nanoparticle diameter and the magnetic field parameter. The similar patterns but opposite effects of heat transfer distribution occur for the increment of the magnetic field and the buoyancy force parameter.*

RÉSUMÉ. *Le but de cette étude est d'étudier le transfert thermique d'un écoulement de l'eau d'oxyde de cuivr nanofludique à l'intérieur d'une une cavité annulaire concentrique entre un carré plus froid et un cylindre elliptique creux utilisant un modèle dynamique non homogène numériquement. La température uniforme est appliquée au cylindre elliptique et à la paroi carrée. Un champ magnétique invariant est imposé dans une enceinte. Les équations de quantité de mouvement, d'énergie et de concentration ainsi que les équations de continuité des nanofluides sont fortement couplées, non linéaires et résolues à l'aide de la méthode des éléments finis de Galerkin. Les champs d'écoulement, thermique et de concentration ont été affichés pour reconnaître le transfert thermique de l'eau d'oxyde de cuivr nanofludique. La nature du transfert thermique est justifiée pour les paramètres pertinents du problème. Les résultats montrent que l'écoulement, le champ thermique et le champ de concentration sont fortement contrôlés par le champ magnétique appliqué. Le transfert thermique augmente de manière significative pour l'augmentation de la fraction volumique de nanoparticules, du nombre de Rayleigh thermique et légèrement pour l'angle d'inclinaison du champ magnétique, alors qu'il diminue de façon notable pour une augmentation du diamètre des*

nanoparticules et du paramètre de champ magnétique. Des schémas similaires et des effets opposés de la répartition du transfert thermique se produisent pour l'incrément du champ magnétique et le paramètre de force de flottabilité.

KEYWORDS: *finite element method, nanofluid, nanoparticles, solar collector, heat transfer.*

MOTS-CLÉS: *méthode des éléments finis, nanofluide, nanoparticules, capteur solaire, transfert thermique.*

DOI:10.3166/ACSM.41.239-260

1. Introduction

The several types of design in the industrial application have been given an enormous attention due to its importance in heat transfer covering for the past few decades. The multiple designs of the annulus-shaped of the enclosures are testing in the multidisciplinary research for the optimal results. There are huge potentialities as well as applications of the annulus shape cavities. As for example, the heat passes through the vacuums inside, of a vessel surrounded by the fluid so that the heat can be transferred smoothly from the source to the outer surface. In the nuclear power plant, the huge generating heat passes through the tube and this can be damaged immediately when the produced heat from the cradle pass across the susceptible surface of the pipe if there is no fluid surrounded over it. Also, in the geothermal energy extraction, the design of the pipe filled with fluid is an annulus shaped. Nowadays, different shapes of the several applications such as batteries, computer appliances, industrial gadgets, and solar thermal technological instrumentation are accessible commercially for heat transfer and cooling intent. To find the maximum heat transfer and cooling operation, the investigations are happening in great numbers and the research on this field increases over the decades in the scientific and engineering communities. The foremost aim is to accomplish the highest heat transfer rate in the applications.

Also, scientists have given huge standing on the convection mode of heat transfer because it occurs in the real-life phenomena as well as in the industrial applications. Specifically, the buoyancy-driven convection is a central focus of many issues since it occurs in many applications such as in the vessels filled with fluids has been applied to cool the radiator, nuclear reactor tor, electronic machineries and devices (de Vahl Davis, 1983; Omri *et al.*, 2005; Tzeng *et al.*, 2005). On the other hand, the conventional fluids such as air, water, acetone, ethylene glycol, and kerosene are using in the practical applications cannot fulfill the requirements to get the finest outcomes. The conventional fluids have low thermal conductivity and other thermophysical properties of them are not optimal. Nowadays, the fluids of higher thermal conductivity are the basic requirement in the applications. So, to adjust with prerequisite the mathematicians, physicists and engineers have suggested nanofluids which are formed by steadily mixing by means of the nanoparticles with the conventional fluids. Nanofluids have higher thermal conductivity and optimal thermal properties which can help to get the optimal heat transfer rate. The exhibition of optimal heat transfer rate using nanofluids in many experiments is available in the literature, for example, Xuan and Li (2003), Wen and

Ding (2004), Buongiorno (2006), Tiwari and Das (2007). The basic understandings along with many advantages, rheological applications and researches of nanofluids are accessible in Uddin *et al.* (2016).

There are many inquiries available in the literature regarding the buoyancy-driven natural convective heat transfer using nanofluids. Using aluminum-water nanofluid, Lai and Yang (2011) conducted an investigation of the natural convective heat transfer in a square-shaped cavity. They investigated the efficiency of this specific nanofluid for two different conditions such as the fixed Rayleigh number and the fixed temperature difference. The outcomes of their investigation are that the typical heat transfer rate enhances for the upsurge of the amount of nanoparticle and the thermal Rayleigh number. However, the deviations of the Nusselt number has been shown as a nonlinear distribution in the work of Tiwari and Das (2007). They have explored the heat transfer proliferation in a square cavity employing nanofluids. Also, they have shown the circumstances and regimes of where the flow of nanofluid changed from the natural convection to forced convection due to the addition of the nanoparticles. The natural thermal cooling of a local thermal origin at the backside of the triangular form occupied with packed nanoparticles is studied by Ghasemi and Aminossadati (2010), and experienced that the add-on of nanoparticles to unpolluted water makes better cooling operation, particularly in a low thermal Rayleigh figure. Using copper-water nanofluid, Soleimani *et al.* (2012) have studied the natural convection in a semi-annulus shaped geometry. Their result shows that there is an optimal angle for the geometry to get the maximum heat transfer. Also, using alumina-water nanofluid, Sheikholeslami *et al.* (2013) have analyzed the natural convection heat transfer in a half-annulus shaped geometry and found that the heat transfer enhancement gains for enhances of the magnetic field parameter and the opposite result are found for the increases of the buoyancy parameter. Also, Sheikholeslami and Abelman (2015) studied the heat transfer in the two horizontal coaxial cylinders using two-phase model and found that the heat transfer is controlled by the different parameters and the width and the hight of the geometry of the problem.

The huge effort has been given to theorizing nanofluid. The first modeling of nanofluids is given by Xuan and Roetzel (2000) to theoretically analyze the convection heat transfer. Another nanofluid model called particle migration modeling has established excellently by Ding and Wen (2005). The two-component mathematical model describing nanofluid with nanoparticle and fluid continuity equations has been given by Buongiorno (2006). Xu *et al.* (2009) have studied buoyancy-driven heat transfer numerically using one-component in a concentrical annulus where the inner wall was the triangular shaped. They proposed the correlations of the mean Nusselt number using the curve matching analysis. Their result shows that the fixed radius ratio, as well as the tilted geometry angle of the annulus, has an insignificant effect on the heat transfer. Sheremet and Pop (2015) have the studied two-component model. It is found that the Brownian motion of nanoparticles and the particle migration is very important to describe nanofluids. One-component model is also used to describe the behaviors of nanofluids widely. Khanafer *et al.* (2003) have inspected mathematically the consequence of nanofluid

supposing that the nanofluid is in solo phase and conveyed that heat transmission rate has been upgraded because of the upsurge of nanomaterial. Sunu *et al.* inspected experimentally the heat transfer in an annulus where the two-heat exchanger with a four-sided corrugated wall has been considered. Throughout their experiment, the shape of the inner tube is tested and found that the grooved wall has a significant effect on the heat transfer. Also, it is found that the heat transfer is remarkably higher for higher Reynolds number compared to the lower one. Siavashi (2015) have used the two-phase mixture model to conduct the numerical study of the alumina-water nanofluid flow features in an annulus. In this investigation, two novel parameters, configuration number, and performance number are introduced. The performance number is decided as the proportion of heat transfer to the pressure departure. According to the configuration number, the performance number is tested for Renolds number and found a significant effect. Using dynamic nonhomogeneous model, Uddin *et al.* (2016b) have studied the heat transfer rate in nanofluids filled different shapes of enclosures. They have shown the uniform level of concentrations for 1-20 nm diameter of nanoparticles in the mixture. The better heat transfer coefficients are calculated and compared with experimental investigations in their studies.

From the aforementioned consequences, it becomes clear that the annulus-shaped vessel is significant in the performance. In addition, various types of vessels (Bhagoria *et al.*, 2002) have been studied on the basis of the many advantages of using nanofluids in the annulus. The main purpose of the present paper is to check the effect of nanofluid filled annulus on the operational geometry where the inner wall is elliptic. Obviously, the dynamically-modeled CuO-water nanofluid-filled wirelessly-shaped vessel, which is not considered to be an unvarying frontier state, is still not studied yet. This numerical modeling is put through with a precise finite element technique, and the actual performance results are illustrated in the form of streamlines, isotherms, and isoconcentrations, where the local Nusselt number dispersions for the pertinent constants of the problem is displayed graphically.

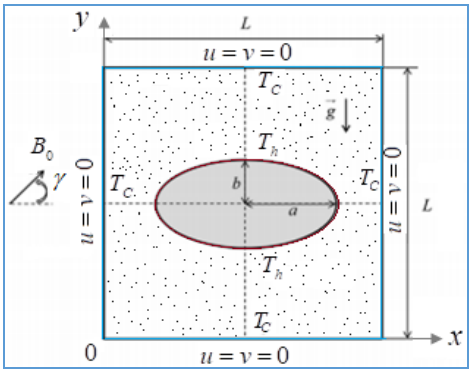

Figure 1. Schematic of the problem

2. Problem formulations

2.1. Physical modeling

The physical model of the problem is displayed in Figure 1, where x and y are Cartesian coordinates. This is designed according to the problem of practical applications. The annulus between a square an ellipse containing copper oxide-water nanofluid has been placed in the coordinates with a minor axis of an ellipse *b* and semi-major axis a where the length of the square-shaped vessel is, *L*. The no-slip conditions for velocity are declared on the boundary walls. Also, the inner elliptical wall of the cavity is a hotter wall and modeled as $T=T_h$ while the outer wall of the annulus is a comparatively colder wall, postured as $T=T_C$, wherever $T_h>T_C$. The existence of the nanofluid concentration is within the entire enclosure whereas there is no concentration available at the boundaries nevertheless avoiding the singularities of the solution, it is assumed that $C=C_h$ on all the boundaries. However, primarily, it is presumed that nanofluid concentration is set aside at stumpy concentration C_C but for $t>0$, it is assumed as C_h in the whole domain such that $C_h>C_C$. A uniform magnetic field, $\mathbf{B} = B_x\hat{e}_x + B_y\hat{e}_y$ is considered within the experiment where the unit vectors $\hat{e}_x$, $\hat{e}_y$ along with the coordinate axes and $B_0^2 = B_x^2 + B_y^2$. The magnetic field's direction creates an angle γ with the positive x-axis. The variations of the thickness of the semi-circular annulus in presence of the magnetic field will be analyzed in the present problem.

2.2. Mathematical modeling

2.2.1. Conservation equations for nanofluid

The nonhomogeneous dynamic model is applied to describe the flow mechanisms of copper water-nanofluid inside the annulus. In the present problem, the radiation and chemical reaction are not included for minimizing the computational complexities whereas the Brownian, thermophoretic diffusion, and temperature and concentration differences due to natural gravitational effects are included through the model. It is assumed that the molecules of conventional fluid and the nanoparticles are an equilibrium in the mixture. The molecules and nanoparticles are the species of the nanofluid because nanoparticles are very tiny, simply can be fluidized. The two-dimensional nonhomogeneous dynamic governing (continuity, momentum in x-direction, momentum in y-direction energy and concentration) equations are as follows:

$$u_x + v_y = 0 \tag{1}$$

$$\rho_{nf}(u_t + uu_x + vu_y) = -p_x + \mu_{nf}(u_{xx} + u_{yy}) + \sigma_{nf}B_0^2\left(v\sin(\gamma)\cos(\gamma) - u\sin^2(\gamma)\right) \tag{2}$$

$$\rho_{nf}(v_t + uv_x + vv_y) = -p_y + \mu_{nf}(v_{xx} + v_{yy}) + (\rho\beta)_{nf} g(T - T_c) + (\rho\beta^*)_{nf} g(C - C_c) + \sigma_{nf} B_0^2 \left(u \sin(\gamma) \cos(\gamma) - v \cos^2(\gamma)\right) \quad (3)$$

$$T_t + uT_x + vT_y = \alpha_{nf}(T_{xx} + T_{yy}) + D_B C^{-1}(C_x T_x + C_y T_y) + D_T T^{-1}[(T_x)^2 + (T_y)^2] \quad (4)$$

$$C_t + uC_x + vC_y = D_B\left(C_{xx} + C_{yy}\right) + C D_T T^{-1}\left(T_{xx} + T_{yy}\right) + D_T T^{-1}\left(C_x T_x + C_y T_y\right) \quad (5)$$

The equations (1-5) respectively are the nanofluid continuity equation, momentum equation in x-direction, momentum equation in y-direction, the nanofluid energy equation, and the nanofluid concentration equation. Here, u and v, p, g, T, T_C, C and C_C respectively are the velocities, pressure, gravity, temperature, reference temperature, concentration and the reference concentration of nanofluid. Also, μ_{nf}, ρ_{nf}, $\alpha_{nf}=k_{nf}/(\rho c_p)_{nf}$, $(\rho c_p)_{nf}$, k_{nf}, $(\rho\beta)_{nf}$ and $(\rho\beta^*)_{nf}$ are the dynamic viscosity, density, thermal diffusivity, thermal conductivity, heat capacity, volumetric thermal expansion and volumetric mass expansion of nanofluid. The applied magnetic field is included with the x- momentum and y-momentum equations. The last term of equations (2) and (3) is the expression of the magnetic field where the nanofluid velocity (v) and the functional magnetic field (**B**) generates a Lorentz force, $\mathbf{J_E}\times\mathbf{B}$, where $\mathbf{J_E}=\sigma_{nf}(\mathbf{E}+\mathbf{v}\times\mathbf{B})$, **E** is the electric field and σ_{nf} is the electrical conductivity. We have a two-dimensional magnetic field, $\mathbf{B}=(B_0\cos\gamma,\ B_0\sin\gamma,\ 0)$ where the orientation angle for the direction of the magnetic field is γ with the horizontal axis and a constant magnitude is B_0 where $B_0 = \sqrt{B_x^2 + B_y^2}$. Let us consider the nanofluid velocities $\mathbf{v}=(u, v, 0)$ and an electric field $\mathbf{E}=0$ where we assumed that the surface is not able to conduct electricity or sound. Therefore the Lorentz forces for x-direction and the y-direction can be calculated respectively are as follows:

$$\sigma_{nf} B_0^2 \left(v \sin(\gamma)\cos(\gamma) - u \sin^2(\gamma)\right) \quad (6a)$$

$$\sigma_{nf} B_0^2 \left(u \sin(\gamma)\cos(\gamma) - v \cos^2(\gamma)\right) \quad (6b)$$

The special electrical conductibility equation for a nanofluid is found from the popular electric conductivity relation of the mixture which is given by Maxwell (1873) is as follows:

$$\sigma_{nf} = \sigma_{bf} \frac{2\sigma_{bf} + \sigma_p - 2\phi(\sigma_{bf} - \sigma_p)}{2\sigma_{bf} + \sigma_p + \phi(\sigma_{bf} - \sigma_p)} \quad (6c)$$

Since there is no clear evidence on which correlation of the nanofluidic properties gives precise results, the most difficult task in the nanofluid problem simulation is the calculation of thermophysical properties, nevertheless, the viscosity of nanofluid is assessed by the standing association for the mixture of two

components. Even though there are lots of research about the thermophysical properties of nanofluidic, the representative thermophysical properties equations are as:

$$\mu_{nf} = \mu_{bf}(1-\phi)^{-2.5} \tag{7}$$

$$\rho_{nf} = (1-\phi)\rho_{bf} + \phi\rho_p \tag{8}$$

$$\left(\rho c_p\right)_{nf} = \phi(\rho c_p)_p + (1-\phi)(\rho c_p)_{bf} \tag{9}$$

$$\left(\rho\beta\right)_{nf} = (1-\phi)(\rho\beta)_{bf} + \phi(\rho\beta)_p \tag{10}$$

$$\left(\rho\beta^*\right)_{nf} = (1-\phi)(\rho\beta^*)_{bf} + \phi(\rho\beta^*)_p \tag{11}$$

$$\kappa_{nf} = \kappa_{bf}\frac{(n-1)\kappa_{bf} + \kappa_p - (n-1)\phi(\kappa_{bf} - \kappa_p)}{(n-1)\kappa_{bf} + \kappa_p + \phi(\kappa_{bf} - \kappa_p)} + \frac{\rho_p c_p \phi}{2}\sqrt{2k_B T_C (3\pi\mu_{nf} d_p)^{-1}} \tag{12}$$

$$D_B = \frac{k_B T_C}{3\pi\mu_{nf} d_p} \tag{13}$$

$$D_T = 0.126\frac{\kappa_{nf}}{\kappa_{bf}}\frac{\lambda\beta_{bf}\mu_{nf}}{\rho_{nf}} \tag{14}$$

where, ϕ is the solid volume fraction, where, k_B is the Boltzmann constant, d_p is the diameter of a nanoparticle, β_{bf} is the thermal expansion of the bulk fluid and the symbol λ is the correction factor depends on the size and shape of the particles as $\lambda = -0.0002d_p + 0.1537$. Here, n=3/Ψ, where Ψ is the sphericity defined as the ratio between the surface area of the sphere and the surface area of the real particle with equal volumes. Also, experimentally proven that *n*=3, *n*=3.7, *n*=4.9, *n*=5.7 and *n*=8.6 represents sphere, brick, cylinder, platelet, and blade shape nanoparticle respectively.

Also, the appropriate initial and boundary conditions of the annulus-shaped enclosure are as follows:

For *t=0*, entire domain:

$$u = v = 0,\ T = T_C,\ C = C_h \tag{15a}$$

For *t>0*, on the inner elliptical wall:

$$u = v = 0,\ T = T_h,\ C = C_h \tag{15b}$$

On the outer square wall:

$$u = v = 0,\ T = T_C,\ C = C_h \tag{15c}$$

2.2.2. Non-dimensional governing equations

The alteration of the equations of dimensional governments in a non-dimensional set of coupled equations is a common practice in the investigation of fluid dynamics. This is also important because transport tools can be easily described by this process. There are some benefits to make them non-dimensional, such as flow monitoring parameters of the problem can be easily identified, there is no dimensional barrier and the results can include any shape and magnitude of the geometry. Therefore, by obtaining the advantages mentioned above, equations (1)-(5) can be transformed into non-dimensional equations, for the following relations without dimension:

$$U = \frac{uL}{\alpha_{bf}}, V = \frac{vL}{\alpha_{bf}}, X = \frac{x}{L}, Y = \frac{y}{L}, \theta = \frac{T - T_C}{\Delta T}, \mathrm{P} = \frac{pL^2}{\rho_{bf}\alpha^2{}_{bf}}, \xi = \frac{\alpha_{bf} t}{L^2}, \Phi = \frac{C - C_C}{\Delta C} \tag{16}$$

where, ξ represents the non-dimensional time, t is the dimensional time, α_{bf} is the base fluid's diffusivity, L is the positional measurement of the geometry, $\Delta T = T_h - T_C$ is the temperature difference, $\Delta C = C_h - C_C$ is the concentration difference within the nanofluid, T_C is applied nominal temperature and C_C is the nominal reference concentration for nanofluid. Using the equation (16) and be familiar with $(\Delta C/C_C) << 1$ and $(\Delta T/T_C) << 1$, the governing equations (1)-(5) can be written dimensionless form respectively as:

$$U_X + V_Y = 0 \tag{17}$$

$$\begin{aligned} U_\xi + UU_X + VU_Y &= -\frac{\rho_{bf}}{\rho_{nf}} P_X + \frac{\mu_{nf}}{\nu_{bf}\rho_{nf}} \mathrm{Pr}(U_{XX} + U_{YY}) \\ &+ \frac{\sigma_{nf}}{\sigma_{bf}} \mathrm{Pr}\, Ha^2 \left(V \sin(\gamma)\cos(\gamma) - U \sin^2(\gamma)\right) \end{aligned} \tag{18}$$

$$\begin{aligned} V_\xi + UV_X + VV_Y &= -\frac{\rho_{bf}}{\rho_{nf}} P_Y + \frac{\mu_{nf}}{\nu_{bf}\rho_{nf}} \mathrm{Pr}(V_{XX} + V_{YY}) + \frac{(\rho\beta)_{nf}}{\beta_{bf}\rho_{nf}} Ra_T \,\mathrm{Pr}\,\theta + Ra_C \,\mathrm{Pr}\,\Phi \\ &+ \frac{\sigma_{nf}}{\sigma_{bf}} \mathrm{Pr}\, Ha^2 \left(U \sin(\gamma)\cos(\gamma) - V \cos^2(\gamma)\right) \end{aligned} \tag{19}$$

$$\theta_\xi + U\theta_x + V\theta_y = \frac{\alpha_{nf}}{\alpha_{bf}}\left(\theta_{XX} + \theta_{YY}\right) + \frac{\left(\Phi_X\theta_X + \Phi_Y\theta_Y\right)}{Le} + \frac{\mathrm{Pr}\, N_{TBT}\left(\left(\theta_X\right)^2 + \left(\theta_Y\right)^2\right)}{Sc} \tag{20}$$

$$\begin{aligned} \Phi_\xi + U\Phi_X + V\Phi_Y &= \mathrm{Pr}\, Sc^{-1}\left(\Phi_{XX} + \Phi_{YY}\right) + \mathrm{Pr}\, Sc^{-1} N_{TBTC}\left(\theta_{XX} + \theta_{YY}\right) \\ &+ \mathrm{Pr}\, Sc^{-1} N_{TBT}\left(\Phi_X\theta_X + \Phi_Y\theta_Y\right) \end{aligned} \tag{21}$$

Here, equations (17)-(21) are respectively called dimensionless nanofluid continuity equation, momentum equations in X-and Y-component, energy equation, and molar concentration equation. The non-dimensionless parameters appeared in the above equations are called, $Ra_T = L^3\beta_{bf}\, g\Delta T(\nu_{bf}\alpha_{bf})^{-1}$ is the thermal Rayleigh number, $Ra_C = L^3 g\Delta C(\rho\beta^*)_{nf}(\nu_{bf}\alpha_{bf}\rho_{nf})^{-1}$ is the solutal Rayleigh number, $\Pr = \nu_{bf}(\alpha_{bf})^{-1}$, is Prandtl number, $Ha^2 = L^2\sigma_{bf}B_0^2(\nu_{bf}\rho_{bf})^{-1}$ is the Hartmann number, $Le=\kappa_{bf}C_C((\rho c_p)_{bf}D_B\Delta C)^{-1}$ is the modified Lewis number, $N_{TBT}=D_T\Delta T(D_B T_C)^{-1}$ is the dynamic thermo-diffusion parameter, $N_{TBTC}=D_T(D_B\Delta CT_C)^{-1}\Delta TC_C$ is the dynamic diffusion parameter, $Sc=\mu_{bf}(\rho_{bf}D_B)^{-1}$ is the Schmidt number.

Also, the initial and boundary conditions in the dimensionless form for the present problem along with the above-stated model can be written as:

For $\xi=0$, entire domain:

$$U = V = 0, \quad \theta = 0, \ \Phi = 1 \tag{22a}$$

For $\xi>0$, On the inner elliptical wall:

$$U = V = 0, \quad \theta = 1, \ \Phi = 1 \tag{22b}$$

On the outer square walls:

$$U = V = \theta = 0, \ \Phi = 1 \tag{22c}$$

3. Computational procedures

The Galerkin Moderate Element Method weighing residual scheme was used in conjunction with the boundary conditions (22) for the management of key equations (17) to (21). Analytical descriptions of this arithmetical method can be found in the book of Zienkiewicz *et al.* (2005) and the Codina's study (1998). The step-by-step procedure of this digital method on the main equations of this problem can be found in the study of Uddin and Rahman. With this method, the domain is restrained in the finite elements consisting of non-triangular elements. Six knots triangular elements are used for the equations of finite element. Then, non-linear partial differential equations are transported to the system of integral equations by enforcing the Galerkin weighted enduring technique. The integration intricate to each of the calculations is completed by the exact integration method. Using the boundary and initial conditions, the obtained non-linear equations must be changed. The iteration technique of Newton-Raphson has been adapted to the term derivative of the Newton Raphson equation to solve the set of global nonlinear algebraic equations as a matrix, and the Euler implicit method to solve the global array. A PDE solver linked with the interface of MATLAB is used to solve the whole physical system along with the governing equations. The results convergence criteria is set to $|I^{m+1}-I^m|\leq 10^{-5}$ here I represents the variables U, V, θ, Φ and m represents the iteration number.

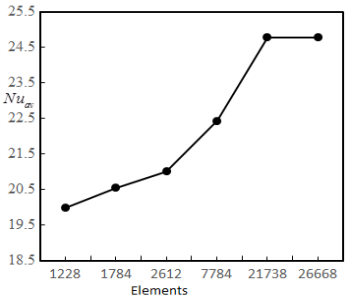

Figure 2. Grids of the enclosure vs average nusselt number

3.1. Grid independence test

It is important to find the number of grids which indicates the results are the independent of a number of the elements for the geometry. Using the thermophysical properties of copper-oxide-water nanofluid and fixing the following values of the parameter: $Ra_C=10^4$, $Ra_T=10^6$, Ha=100, γ=0°, d_p=10nm, $\phi=0.05$, n=3 and $\xi=1$, the several number elements in an annulus in terms the average Nusselt number have been tested. We have examined six unlike non-undifferentiated control grid structures with the following number of elements: 1228, 1784, 2612, 7784, 21738 and 26668. The average Nusselt number for the aforesaid number of grids is calculated from the heated elliptic inner wall of the annulus which is shown in Figure 2. It is observed from the figure that the value of the average Nusselt number for the element, 21738 is almost the same as that of the elements, 2668. In this case, we have taken 21738 elements to display our results and the results are independent of a number of grids.

Table 1. Comparisons of the present numerical data in terms of average Nusselt number with that of the results of Saghir et al. (2016) and Ho et al. (2010)

Studies	Average Nusselt number (Nu_{ave})		
	$\phi=1\%$	$\phi=2\%$	$\phi=3\%$
Ho et al. (2010)	31.8633	31.6085	28.2160
Saghir et al. (2016)	32.2037	31.0905	29.0769
Present result	32.1900	31.0354	28.9580

3.2. Code validation

Two benchmark studies such as the numerical study of Saghir *et al.* (2016) as well as the experimental work of Ho *et al.* (2010) have been considered to test the present code of the problem. The comparisons are displayed in Table 1. We have

used our present code for an absolute benchmark study of Saghir *et al.* (2016). The governing equations, the physical relations, the type of nanofluid and the geometry of this study are used for the present code to display the comparative results. The results are calculated by the following empirical equation of the mean Nusselt number:

$$Nu_{ave} = 0.069\ [\beta_{nf,h}(\beta_{nf})^{-1}]^{0.404}\ [\mathrm{Pr}_{nf,h}(\mathrm{Pr}_{nf})^{-1}]^{0.333} \tag{23}$$

Here, $\beta_{nf,h}(\beta_{nf})^{-1}$, represents the proportion of the thermal expansion of nanofluid at hot temperature and that of the mean temperature. Also, $Pr_{nf,h}(Pr_{nf})^{-1}$ represents the ratio of the Prandtl number which is quantified for alumina oxide -water nanofluid at the hot temperature to the Prandtl number of the same nanofluid at the average temperature of 26 degree Celsius and the temperature difference of 12 degree Celsius. The equation (23) is used to compare the benchmark studies with the present investigation. The outcomes in terms of the mean Nusselt number for different solid particle volume fraction have been compared and shown in Table 1. It is found that the values of mean Nusselt number for several solid volume fractions from our numerical code have reflected the similar results with benchmark numerical studies and with the experimental outcomes. These analogous consequences are heartened us to show and deliberate more solutions to the problem.

4. Results and discussions

The thermophysical properties of copper-oxide nanoparticle and the base fluid like water is implemented for discussing the results. In the problem design, some parameters are defined by the values of the physical characteristics. The thermophysical belongings of water are: κ_{bf}=0.613 $Wm^{-1}K^{-1}$, ρ_{bf}=997.1 kg m^{-3}, $(c_p)_{bf} = 4179\ Jkg^{-1}K^{-1}$, $\sigma_{bf} = 5.5\times10^{-5}\ Sm^{-1}$, $\beta_{bf} = 21\times10^{-5}\ K^{-1}$, $\mu_{bf} = 0.001003$ $kgm^{-1}s^{-1}$. The properties of copper-oxide nanoparticle are: κ_p=76.5 $Wm^{-1}K^{-1}$, ρ_p=6320 kg m^{-3}, $(c_p)_p = 531.8\ Jkg^{-1}K^{-1}$, $\sigma_p = 59.6\times10^{6}\ Sm^{-1}$, $\beta_p = 1.8\times10^{-5}\ K^{-1}$. Also, to define the values of the parameters, we have well-thought-out some standard values such as: $\Delta C=0.01$, $\Delta T=10K$, Tc=300K, dp=10nm, C_C=1, n=3, and $\phi = 0.05$. Using the above-mentioned values, some sample values of the physical parameters arrived into the dimensionless governing equations for the copper oxide-water nanofluids are as follows: Sc=26111, N_{TBT}=0.0075495, N_{TBTC}=0.75495, Le=3.82×10^{5}, D_T=8.725×10^{-12} and D_B=3.8525×10^{-11}. On the other hand, the Hartmann number, the thermal Rayleigh number, the solutal Rayleigh number, and the magnetic field inclination angle are changed to investigate the heat transfer of the current problem. Nanofluid is a mixture of a normal fluid and the solid particles. So, the characteristics of nanofluids are absolutely depended on the characteristics of base fluids and types of nanoparticles. Also, the parameters entered into the problem depend on that of the types, amount of base fluids, solids as well as the size of the solids.

The numerical results in terms of the free convective heat transfer in an annulus containing nanofluid are discussed in this division. In the simulation, the properties of copper-oxide and water are used to explain the thermal, flow, concentration fields and the local Nusselt number distribution. The important features like the effects of the nanoparticle volume fraction, the nanoparticle length and the shape of nanoparticles using copper-oxide-water nanofluid on the heat transfer application are the main focus of the current investigations. The ratio of two different buoyancy-parameter used in the study is secured to 100. The flow fields in terms of streamlines, the thermal fields in terms of isotherms, and uniformity of the solid particles in terms of the isoconcentrations for several pertinent parameters are displayed to analyze the problem. The distinction of the local Nusselt number at the heated internal surface of the vessel for the Hartmann number, Rayleigh number, nanoparticle sizes, volume fraction as well as, magnetic field tilted angle and shape factors of nanoparticle have been displayed graphically. The concise but adequate clarification tracks apiece result.

Figure 3 displays the Streamlines (left column) and isotherms (right column) distributions for $Ra_T=10^5$ (top row), $Ra_T=10^6$ (middle row) and $Ra_T=10^7$ (bottom row) for fixed values of $\phi=0.05$, dp=10nm, Ha=100, n=3, $\gamma=0^0$ at $\xi=1$ (steady state). As can be seen from the left column of the figure that that two rotational big vortices are significantly strong inside the enclosure throughout the cases.

There are two small but strong vortices also visible inside each of big vortex which indicates the strong flow of nanofluid in the annulus. Also, it is important to note that the directions of the vortices are opposite to each other. The cells of vortices are formed in a symmetric manner showing very normal nature of convection. This intends that the flow decorations are symmetrically distributed in the objects.

This happens due to the presence of the horizontal elliptical inner walls inside the square enclosure and the heat transfers through the elliptical shape of heat source uniformly to nanofluid in the annulus. Fluid takes heat energy from the inner elliptic wall uniformly and becomes lighter to prompt a convective current to the square walls. Lighter fluid goes up and the colder portion of fluid follows the line traced by the colder wall due to the symmetric nature of the square colder walls. As a consequence, symmetric cells within the two vortices are obtained. Also, as the thermal Rayleigh number increases, the strength of the flow field upsurges.

For the lower value of thermal Rayleigh number, the densities of streamlines are not that much pronounced. Also, the values of maximum surface velocities are very low in this case showing poor convective heat transfer. However, for higher values of thermal Rayleigh number, streamlines are vigorously visible in the entire enclosure and maximum surface velocities are optimal. This indicates the advanced flow fields. This is due to the fact that the higher temperature differences occurred for higher values of thermal Rayleigh number which makes the optimal random collations, migrations, and motion of the nanoparticles in the annulus. From the right column of Figure 3, we have seen that the isotherms are very strong and significantly distorted for the higher values of thermal Rayleigh number. The heat

goes to upwards and spreads almost in the entire enclosure excellently in this case. The thickness of the thermal boundary layer on the walls is not that much significant due to the high-temperature gaps. This indicates strong convection mode of heat transfer in the applications. Whereas for the lower values of the thermal Rayleigh number, the isotherms are not considerable distorted, they are compressed to the elliptical wall, and they are almost parallel to the heated wall. The thickness of the thermal layer on the heated boundary is significant in this case. This indicates that the conduction mode of heat transfer controls in the vessel. This occurs because of the lesser temperature differences change within the annulus.

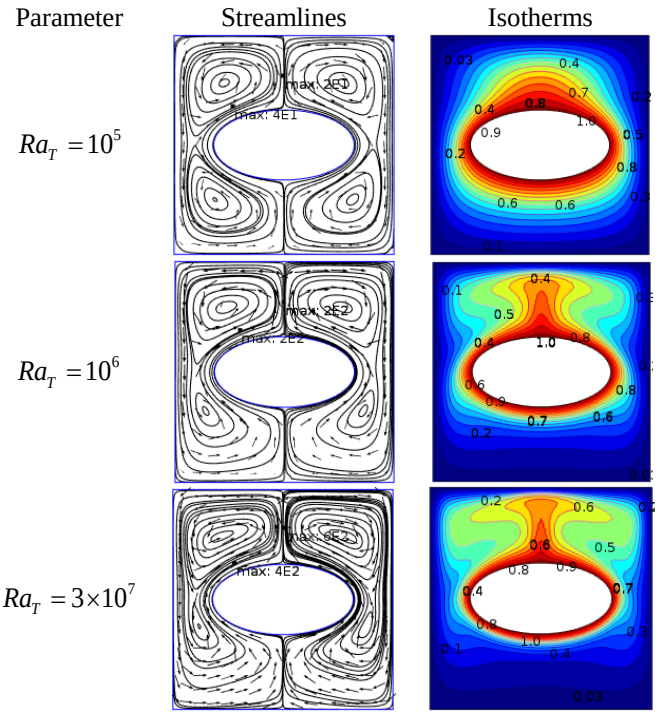

Figure 3. Streamlines (left column) and isotherms (right column) distributions for $Ra_T=10^5$ *(top row),* $Ra_T=10^6$ *(middle row) and* $Ra_T=3\times10^7$ *(bottom row) for fixed values of* $\phi=0.05$, $d_p=10nm$, $Ha=100$, $n=3$, $\gamma=0^0$ *at* $\xi=1$

Figure 4 illustrates the effect of the thermal Rayleigh number on the isoconcentrations of nanofluid for different values of thermal Rayleigh number at $\xi=0.1$ (left column) and at $\xi=1$ (right column). It is clear that the pattern and the state of the isoconcentrations change pointedly over the periods of time. The strengths and levels of isoconcentrations increase for the time $\xi=1$ than that of the time, $\xi=0.1$. At the beginning of the mixing, the nanoparticle has a tendency to cluster on the hotter boundary. This means that initially, nanoparticles take time to

settle down in the base fluid. The particle migrations and the random collisions along with the molecules of the base fluid in this case not in the equilibrium state. Also, the terminal velocity of the particle is not negligible in this case. Over the course of time, the loop of the isoconcentrations become very strong and accelerated the flow that creates the full-bodied loop of isoconcentrations within the annulus. Also, as the thermal Rayleigh number increases, the strength and the levels of the isoconcentrations increases noticeably, the densities of the lines of isoconcentrations in the loops upsurges, and the lines of isoconcentrations spread all the way in the cavity throughout the different stages of times. These happen because of the higher temperature differences in the cavity results in the higher thermal Rayleigh number for which the particle diffusions and random interactions of particles are maximized. Hence, the even dissemination of the tracing of nanoparticles occurs for the higher value of Rayleigh number which indicates the better convection in the enclosure.

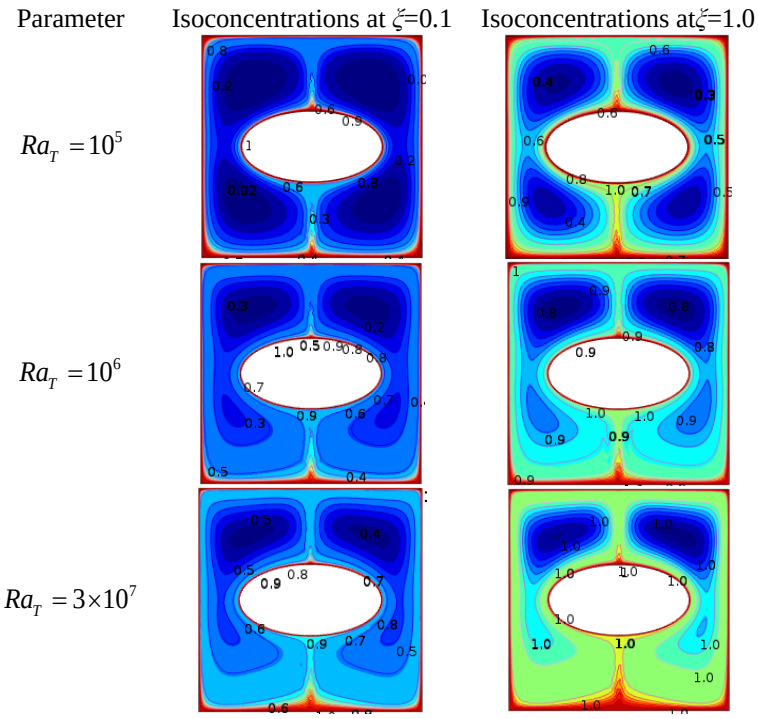

Figure 4. Isoconcentrations at ξ=0.1 (left column) and isoconcentrations at ξ=1 (right column) for $Ra_T=10^5$ (top row), $Ra_T=10^6$ (middle row) and $Ra_T=10^7$ (bottom row) for fixed values of ϕ=0.05, dp=10nm, Ha=100, n=3, γ=0°

Figure 5 represents the effects of the magnetic field parameter on isotherms (right column) and streamlines (left column) for fixing different parameters. It is observed that the magnetic field parameter namely the Hartmann number significantly suppresses and controls the flow field and thermal field. The configurations of the streamlines and isotherms are remarkably influenced by the Hartmann number. This is due to the hydro-magnetized cooper-oxide nanoparticles which have crystallographic construction and demonstrating ferromagnetism behavior.

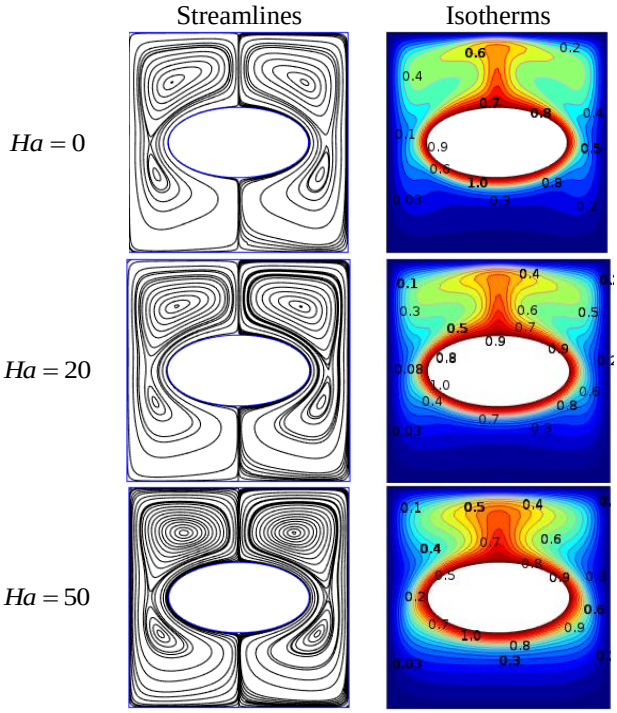

Figure 5. Effect of magnetic field on streamlines (left column) and isotherms (right column) for γ=30° (top row), γ=60° (middle row) and γ=90° (bottom row) with d_p=10nm, ϕ=0.05, Ha=100, n=3 at ξ=1

The vortices inside the enclosure oppositely rotate each other. The rotations within the annulus are comparative lesser in presence of the magnetic field parameter. Also, the pattern of the rotations completely unchanged in presence of the magnetic field compared with the flow field where the magnetic field is not present. However, the densities are increased due to the increased values of the Hartmann number. This is due to the higher intensities of the constant magnitude of the magnetic field. As the value of the magnetic field parameter are increased from *Ha*=0 to *Ha*=50, the strengths of the streamlines and isotherms are decreased, the

intensities of the rotations of the flow inside the enclosure dwindled and the number of vortices and the thermal plumes of isotherms stepped-down. The compact streamlines and suppressed isotherms to the heated elliptical wall within the annulus are observed for *Ha*=50. Also, the level of the isotherms near the boundaries of the colder walls is decreased for the increased values of the Hartmann number. These indicate that the heat transfer in the applications can be controlled and decreased by the magnetic field parameter. The heat transfer in terms of the local Nusselt number dissemination at the heated elliptical shape of a heat source for the different pertinent parameters fixing others related parameters of the problem is displayed in Figure 6.

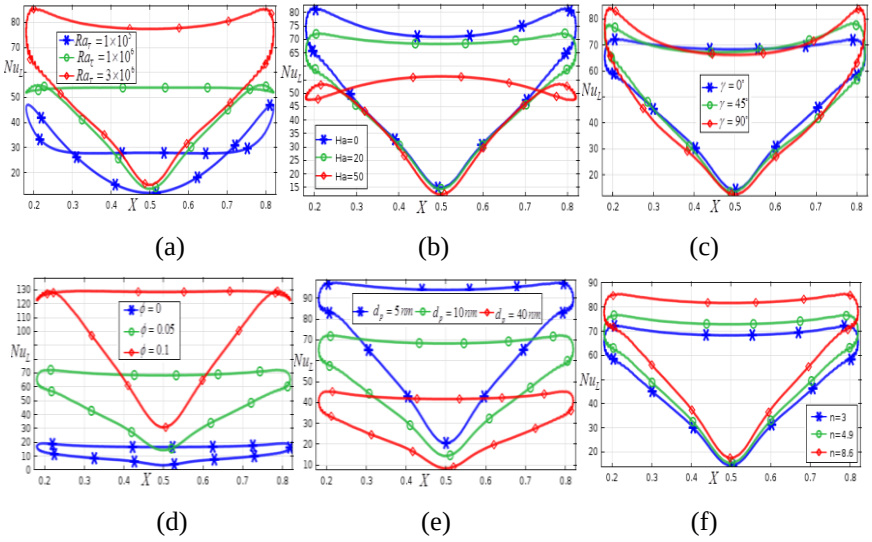

Figure 6. Local Nusselt number versus (a) Rayleigh number (b) Hartmann number, (c) magnetic field inclination angle (d) nanoparticle volume fraction (e) diameter of the particle and (f) shape factors of the particle for the fixed values of ϕ=0.05, Ra_T=1.7×10^6, d_p=10nm, Ha=100, n=3, γ=0° at ξ=1

As can be seen from the figure that the heat transfer distribution significantly molded with the changes of the parameters of the problem. Specifically, from Figure 6(a), we have seen that the local Nusselt number is increased when the thermal Rayleigh number is increased. The three different values of the thermal Rayleigh number are tested. It is found the higher values of the thermal Rayleigh number exhibits significantly higher heat transfer distribution. Also, the pattern of the heat transfer distribution changes with the changes of the thermal Rayleigh number. As Rayleigh number increases the pattern of the local Nusselt number distribution becomes necklace shaped and more panoptic whereas for the intermediate value of the thermal Rayleigh number, it is almost a triangular and for lower values of the

thermal Rayleigh number, it is a zigzag-shaped. These indicate that the highest average heat transfer rate can be found for the higher values of the Rayleigh number.

Nevertheless, the almost reverse pattern of the local Nusselt number distribution can be comprehended by the Figure 6(b) where it represents the heat transfer distribution for different values of the magnetic field parameter. The heat transfer distribution on the heated wall of the vessel is displayed for *Ha*=0-50. As can be observed that as the Hartmann number decreases, the distribution of the local Nusselt number diminutions significantly. Therefore, it is clear that the heat transfer in an application can be modified by the setup of the magnetic field. Also, the pattern of the heat transfer distribution can be controlled using the magnetic field setup.

The effect of the magnetic field inclination angle on the heat transfer distribution is an interesting result in the natural convective heat transfer research. Figure 6(c) represents the effect of the directions of the magnetic field. It is found that the local Nusselt number dissemination augments slightly with the augmentation of the magnetic field tilted angle. In this case, the effects are not that much distinguishable. Explicitly, the swelling tendency of the local Nusselt number distribution is not that much pronounced for $0°\leq\gamma\leq45°$ whereas, for $\gamma=90°$, the heat transfer distribution is noticeably higher than that of the other angles.

The nanoparticle volume fraction versus the local Nusselt number is illustrated in Figure 6(d). As can be found that as nanoparticle volume fraction increases, the local Nusselt number increases noticeably. Also, the heat transfer distribution on the heated wall for nanofluid is significantly higher than that of the base fluid. This is due to the resultant effect of the nanoparticle and the base fluid. A pivotal notice is that the distribution of heat transfer for base fluid where the solid particles are absent is much squeezed, almost a straight line although the heated wall is an elliptical shaped. Nevertheless, for nanofluid, the heat transfer distribution is very wide on the heated elliptical wall and it looks a cone-shaped. This may be due to the movement of the nanoparticles in the fluid which enhances the normal heat transfer distribution. This represents that the stable and average heat transfer can be found utilizing nanofluid compared to that of the base fluid.

Figure 6(e) depicts the heat transfer distribution on the heated wall for different size of the solid particles in the mixture. The significant effect is noticed in this regard. As can be seen from the figure that the heat transfer distribution is seriously declined with the increase in the size of the nanoparticle diameter. This is due to the diffusion nature of the nanoparticles. The Brownian diffusion and the thermophoretic diffusion are reciprocal of the size of the solid particles in the solution. It is important to the mansion that several sizes of the nanoparticles are also tested and the conspicuous decreasing trend in the heat transfer distribution is perceived for *dp*=1-60nm. Also, the prominent modification (declining tendency) of the heat transfer for different size of the nanoparticle is enhanced if the nanoparticle volume fraction is increased. Hence, in the application of nanofluid, it is suggestive to mix up as much as smaller solid particles with the base fluid.

The effects of the shape factors of solid particles of base fluid over the heat transfer distribution are depicted in Figure 6(f). Using the shape factor, the original shape of the solid nanoparticle in the application can be determined. Here, the shape factor 3, 4.9 and 8.6 represents the spherical, cylindrical and blade-shaped of nanoparticles. It is observed that the heat transfer distribution is increased as the shape factor of the nanoparticle is increased. In this case, the spherical shape of nanoparticle shows lowest heat transfer distribution whereas the blade shape of solid particle displays the maximum heat transfer distribution. So, it is essential to note that whenever nanofluids are produced for the heat transfer application, it is better to stably mix up the solid nanoparticles of having highest shape factor with the conventional fluid.

5. Conclusion

The numerical simulation on the natural convective heat transfer flow of nanofluid filled an annulus shaped geometry between a square and ellipse-shaped boundary has been investigated. The temperature of the elliptical inner wall is assumed to be uniformly distributed whereas the outer square wall is assumed to be considerably colder. The numerical results have been demonstrated that the flow field, thermal field and concentration level of nanofluid in the geometry are extremely stricken by the parameters of the problem, the time as well as the shape of the heat source. The magnetic field can control the heat transfer rate and the pattern of the flow. The effect of the direction of the magnetic filled is not much pronounced in this study. The stability of nanoparticles in the solution occurred after certain periods of time. Also, the nanoparticles and the base fluid have taken time to reach the stable and equilibrium state. Also, a significant level of buoyancy force is needed to make a thermal equilibrium solution. In the initial periods of time, the isotherm was unstable and after a certain time, it became stable. The heat transfer distributions are calculated for the different pertinent parameters of the problem. The heat transfer distribution is increased when the thermal Rayleigh number, the nanoparticle volume fraction, the shaped factors of the nanoparticle are increased. On the other hand, the heat transfer distribution is decreased when the applied magnetic field (Hartmann number) and the size of the nanoparticle are increased. The effect of the direction of the magnetic field on the heat transfer distributions is quite positive.

References

Bhagoria J. L., Saini J. S., Solanki S. C. (2002). Heat transfer coefficient and friction factor correlations for rectangular solar air heater duct having a transverse wedge-shaped rib roughness on the absorber plate. *Renewable Energy*, Vol. 25, No. 3, pp. 341-369. https://doi.org/10.1016/s0960-1481(01)00057-x

Buongiorno J. (2006). Convective transport in nanofluids. *Journal of Heat Transfer*, Vol. 128, No. 3, pp. 240-250. https://doi.org/10.1115/1.2150834

Codina R. (1998). Comparison of some finite element methods for solving the diffusion-convection-reaction equation. *Computer Methods in Applied Mechanics and Engineering*, Vol. 156, No. 1-4, pp. 185-210. https://doi.org/10.1016/S0045-7825(97)00206-5

De Vahl Davis G. (1983). Natural convection of air in a square cavity: A benchmark numerical solution. *International Journal for Numerical Methods in Fluids*, Vol. 3, No. 3, pp. 249-264. https://doi.org/10.1002/fld.1650030305

Ding Y., Wen D. (2005). Particle migration in a flow of nanoparticle suspensions. *Powder Technology*, Vol. 149, No. 2-3, pp. 84-92. https://doi.org/10.1016/j.powtec.2004.11.012

Ghasemi B., Aminossadati S. M. (2010). Brownian motion of nanoparticles in a triangular enclosure with natural convection. *International Journal of Thermal Sciences*, Vol. 49, No. 6, pp. 931-940. https://doi.org/10.1016/j.ijthermalsci.2009.12.017

Ho C. J., Liu W. K., Chang Y. S., Lin C. C. (2010). Natural convection heat transfer of alumina-water nanofluid in vertical square enclosures: an experimental study. *International Journal of Thermal Sciences*, Vol. 49, No. 8, pp. 1345-1353. https://doi.org/10.1016/j.ijthermalsci.2010.02.013

Khanafer K., Vafai K., Lightstone M. (2003). Buoyancy-driven heat transfer enhancement in a two-dimensional enclosure utilizing nanofluids. *International Journal of Heat and Mass Transfer*, Vol. 46, No. 19, pp. 3639-3653. https://doi.org/10.1016/s0017-9310(03)00156-x

Lai F. H., Yang Y. T. (2011). Lattice Boltzmann simulation of natural convection heat transfer of Al_2O_3/water nanofluids in a square enclosure. *International Journal of Thermal Sciences*, Vol. 50, No. 10, pp. 1930-1941. https://doi.org/10.1016/j.ijthermalsci.2011.04.015

Maxwell J. A. (1873). A treatise on electricity and magnetism. *Clarendon Press, Oxford*.

Omri A., Orfi J., Nasrallah S. B. (2005). Natural convection effects in solar stills. *Desalination*, Vol. 183, No. 1-3, pp. 173-178. Https://doi.org/10.1016/j.desal.2005.04.025

Saghir M. Z., Ahadi A., Mohamad A., Srinivasan S. (2016). Water aluminum oxide nanofluid benchmark model. *International Journal of Thermal Sciences*, Vol. 109, pp. 148-158. https://doi.org/10.1016/j.ijthermalsci.2016.06.002

Sheikholeslami M., Abelman S. (2015). Two-phase simulation of nanofluid flow and heat transfer in an annulus in the presence of an axial magnetic field. *IEEE Transactions on Nanotechnology*, Vol. 14, No. 3, pp. 561-569. https://doi.org/10.1109/TNANO.2015.2416318

Sheikholeslami M., Gorji-Bandpy M., Ganji D. D. (2013). Numerical investigation of MHD effects on Al_2O_3-water nanofluid flow and heat transfer in a semi-annulus enclosure using LBM. *Energy*, Vol. 60, pp. 501-510. https://doi.org/10.1016/j.energy.2013.07.070

Sheremet M. A., Pop I. (2015). Mixed convection in a lid-driven square cavity filled by a nanofluid: Buongiorno's mathematical model. *Applied Mathematics and Computation*, Vol. 266, pp. 792-808.

Siavashi M., Bahrami H. R., Saffari H. (2015). Numerical investigation of flow characteristics, heat transfer and entropy generation of nanofluid flow inside an annular pipe partially or completely filled with porous media using two-phase mixture model. *Energy*, Vol. 93, pp. 2451-2466.

Soleimani S., Sheikholeslami M., Ganji D. D., Gorji-Bandpay M. (2012). Natural convection heat transfer in a nanofluid filled semi-annulus enclosure. *International Communications in Heat and Mass Transfer*, Vol. 39, No. 4, pp. 565-574. https://doi.org/10.1016/j.icheatmasstransfer.2012.01.016

Tiwari R. K., Das M. K. (2007). Heat transfer augmentation in a two-sided lid-driven differentially heated square cavity utilizing nanofluids. *International Journal of Heat and Mass Transfer*, Vol. 50, No. 9-10, pp. 2002-2018. Https://doi.org/10.1016/j.ijheatmasstransfer.2006.09.034

Tzeng S. C., Liou J. H., Jou R. Y. (2005). Numerical simulation-aided parametric analysis of natural convection in a roof of triangular enclosures. *Heat Transfer Engineering*, Vol. 26, No. 8, pp. 69-79. Https://doi.org/10.1080/01457630591003899

Uddin M. J., Al Kalbani K. S., Rahman M. M., Alam M. S., Al-Salti N., Eltayeb I. (2016a). Fundamentals of nanofluids: Evolution, applications and new theory. *International Journal of Biomathematics and Systems Biology*, Vol. 2, No. 1, pp. 1-32.

Uddin M. J., Alam M. S., Al-Salti N., Rahman M. M. (2016b). Investigations of Natural convection heat transfer in nanofluids filled horizontal semicircular-annulus using nonhomogeneous dynamic model. *Am J Heat Mass Transf*, Vol. 3, No. 6, pp. 425-452.

Wen D., Ding Y. (2004). Experimental investigation into convective heat transfer of nanofluids at the entrance region under laminar flow conditions. *International Journal of Heat and Mass Transfer*, Vol. 47, No. 24, pp. 5181-5188. Https://doi.org/10.1016/j.ijheatmasstransfer.2004.07.012

Xu X., Sun G., Yu Z., Hu Y., Fan L., Cen K. (2009). Numerical investigation of laminar natural convective heat transfer from a horizontal triangular cylinder to its concentric cylindrical enclosure. *International Journal of Heat and Mass Transfer*, Vol. 52, No. 13-14, pp. 3176-3186. Https://doi.org/10.1016/j.ijheatmasstransfer.2009.01.026

Xuan Y., Li Q. (2003). Investigation of convective heat transfer and flow features of nanofluids. *Journal of Heat Transfer*, Vol. 125, No. 1, pp. 151-155. Https://doi.org/10.1115/1.1532008

Xuan Y., Roetzel W. (2000). Conceptions for heat transfer correlation of nanofluids. *International Journal of Heat and Mass Transfer*, Vol. 43, No. 19, pp. 3701-3707. Https://doi.org/10.1016/s0017-9310(99)00369-5

Zienkiewicz O. C., Taylor R. L., Nithiarasu P. (2005). The Finite Element Method for Fluid Dynamics. *6th edition, Elsevier*.

Nomenclature

C	concentration of nanofluid (mol/m^3)
C_c	reference concentration (mol/m^3)
c_p	specific heat (J/kgK)
D_B	Brownian diffusion coefficient (m^2/s)
d_p	diameter of nanoparticle (nm)
D_T	thermal diffusion coefficient (m^2/s)

Ha	the Hartmann number
k_B	Boltzmann constant (J/K)
L	length of the bottom wall (m)
Le	Lewis number
Nu	Nusselt number
Nu_{ave}	average Nusselt number
N_{TBTC}	dynamic diffusion parameter
N_{TBT}	dynamic thermo-diffusion parameter
n	the empirical shape factor of nanoparticles
p	dimensional pressure (Pa)
P	dimensionless pressure
Pr	Prandtl number
Ra_T	local thermal Rayleigh number
Ra_c	local solutal Rayleigh number
Sc	Schmidt number
t	dimensional time (s)
T	temperature (K)
T_h	the temperature of the hot wall (K)
T_c	the temperature of the cold wall (K)
(u, v)	dimensional velocity components (m/s)
(x, y)	dimensional coordinates (m)
(X, Y)	dimensionless coordinates

Greek letters

α	thermal diffusivity (m^2/s)
β	the coefficient of volume expansion (K^{-1})
β^*	the coefficient of mass expansion (K^{-1})
σ	the electric conductivity (Sm^{-1})
τ	nondimensional time
ρ	density (kg/m^3)
μ	dynamic viscosity (Pas)
υ	the kinematic viscosity

θ	dimensionless temperature
ϕ	nanoparticles volume fraction
Φ	dimensionless concentration
k	thermal conductivity (W/mK)
ψ	stream function
Ψ	the sphericity of the nanoparticles
ΔC	concentration drop (mol/m^3)
ΔT	temperature drop (K)

Subscripts

ave	average
bf	base fluid
nf	nanofluid
p	solid nanoparticle